Sixth International Symposium on Turbulence and Shear Flow Phenomena
Seoul, Korea, 22-24 June 2009

IDENTIFICATION OF PERIODIC AND CYCLIC EVENTS IN COMPLEX TURBULENT FLOWS

Sylvain Lardeau
Fabrizio Tessicini
Michael .A. Leschziner
Department of Aeronautics,
Imperial College London
South Kensington Campus, London, SW7 2AZ, United Kingdom
s.lardeau@imperial.ac.uk

ABSTRACT

A new technique for extracting information about cyclic and periodic features in turbulent-flow fields is proposed. A phase-space decomposition of the flow field is first performed, based on proper orthogonal decomposition (POD), and then recurrence plots (RPs) are used to analyse the system. The technique allows the temporal behaviour of the flow viewed as a dynamic system to be identified. The basic elements of the analysis are presented first, with the Lorenz system used for illustration, and then two related flows field are analysed with the new technique, with results contrasted against the classical spectral analysis.

INTRODUCTION

There are several well-established approaches to scrutinizing structural features in full-field representations (PIV, DNS, LES) of complex flows - e.g. via a visualisation of the Q, λ_2, pressure, enstrophy fields. However, there are few tools available for analysing periodic, quasi-periodic and cyclic events. Spectra derived from time-series form the usual route to identifying (broadly) periodic events. However, when this periodicity is not well-defined (i.e. is modulated or varies in frequency within a limited range), and when the frequency is low, so that the data available do not span many cycles, spectra return very noisy data and broadband behaviour. POD is an alternative approach, in so far as it yields the temporal coefficients of the eigenmodes of any chosen flow variable, organised according to the energy content of the flow. Here again, the scope for identifying cyclicities is very limited, because this can only be done by analysing the coefficients as separate time-series. This can be misleading if, as is the case in complex turbulent flows, the energy variation across many leading modes is fairly uniform.

Configurations in which quasi-periodic and cyclic events are especially difficult to identify are relatively weakly separated flows, e.g. separation from humps, hills and gently curving ramps of relatively low height-to-length ratios. Typically, the question arises whether there is any kind of regular or quasi-regular "shedding-like" periodicity or flapping, or whether there are cyclic events that occur regularly, but infrequently, and at irregular intervals. Such information is not only fundamentally important, but can have real practical implications associated with characterising extreme events and identifying excursions that can lead to instability and vibrations.

In this paper we apply a recently developed approach (Lardeau et al, 2008) that combines POD with "Recurrence Plots" (RPs), a tool well-established in dynamical-systems analysis outside Fluid Mechanics, to weakly-separated flows. We demonstrate that this approach allows cyclicities to be identified visually from particular patterns in the plots. A supporting quantitative analysis rests on extracting the *probability of recurrence* from the RP. In dynamical-systems terminology, the distinct cyclicities thus identified represent drastic changes of the dynamical system (i.e. global flow) behaviour in phase-space.

PROPER ORTHOGONAL DECOMPOSITION

The starting point of the method is a selected subset (or all) of the relevant "modes" for the flow in question. The temporal coefficients of the modes are held to characterise the evolution of the flow as a dynamical system in a multi-dimensional phase-space. The trajectory in this subspace may display quasi-periodic behaviour, presumed to correspond to related quasi-periodic events in the flow as a whole. Any flow field realisation can be decomposed as

$$u_i(\vec{x},t) = \sum_{n=1}^{N} a_n(t)\phi_i^n(\vec{x}) \qquad (1)$$

where N is the number of modes used for the representation, $a_n(t)$ are temporal modes and $\{\phi_i^n\}$ represent basis functions that need to be selected to comply with a specific criterion upon which the representation of the flow field is desired. For POD, this basis is chosen so as to maximise the energy content of lower-order modes (Holmes *et al.*, 1996). If the flow is unbounded (infinite, periodic) in one direction, here represented by homogeneity in the z-direction, the empirical eigenfunctions can be regarded as plane waves and take the form:

$$\phi_i^n(x,y,z) = \xi_i^q(x,y,k)\exp(-\iota kz) \qquad (2)$$

where q is the so-called quantum number. The behaviour of the system emerges visually from a particular processing of the temporal coefficients and a particular way of plotting the processed results on a Recurrence Plot (RP).

RECURRENCE PLOTS

A RP is a two-dimensional map with both axes being time (Marwan et al., 2007). If the state of the dynamical system at time t_i is characterised by the n-dimensional vector $\vec{x}^i$ (representing its "properties" in some specified sense) and at time t_j by $\vec{x}^j$, a *distance* norm between the two states at the two different times may be computed. This can be done for any time value t_i, associated with one axis of the RP, and any other time value t_j, associated with the other axis. When this distance is below a given threshold ε, the

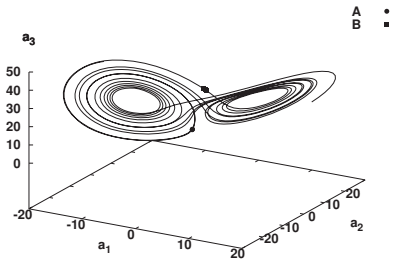

Figure 1: Phase-space trajectory of the Lorenz system, Eq. 8, with $\sigma = 10$, $\beta = 8/3$ and $\rho = 28$.

system (the flow) may be said to be close to the state on a previous time (which is regarded as a recurrence). Mathematically, this can be expressed as:

$$R_{ij} = \theta(\varepsilon - ||\vec{x}^i - \vec{x}^j||) \tag{3}$$

where θ is the Heaviside function. i.e. a value of 1 is then attributed to events at a distance less than ε, and a value 0 identifies events at a distance greater than ε. The value 1 is then entered as a black mark into the RP, while locations corresponding to the value 0 remain white. For non-stochastic processes, the RP features characteristic patterns to which specific meanings can be attributed, as illustrated below. Among many significant features, the most frequent patterns observed are lines parallel to the "Line of Identity" (LOI) - the diagonal of the time-time plot - and horizontal and vertical strips. Continuous or discontinuous lines parallel to the LOI identify the fact that the trajectory visits the same region of the phase-space at different times. The length of any diagonal line is determined by the duration of such a similar local evolution of the trajectory segments.

A more general approach to constructing RPs (refered to as *Global* recurrence plots, GRP) is to use the distance between two points in the phase-space

$$D_{ij} = ||\vec{x}^i - \vec{x}^j|| \tag{4}$$

and sensitise this quantity continuously to gray shading on the GRP. However, Eq. 4 is dimensional, i.e. the range of values that D_{ij} can take depends on the diameter (in the phase-space) of system considered. On the other hand, R_{ij} (Eq. 3) requires a definition of a unique ε and this also depends on the system.

A definition that avoids the two major drawbacks noted above is:

$$U_{ij} = C_2(||\vec{x}^i - \vec{x}^j||) \tag{5}$$

where $C_2(.)$ is called the Grassberger-Proccacia correlation and is defined by:

$$C_2(\varepsilon) = \frac{1}{N^2} \sum_{i,j=1\ ;\ i \neq j}^{N} \theta(\varepsilon - ||\vec{x}^i - \vec{x}^j||) \tag{6}$$

which is a measure of the *recurrence density*, for a given value of the threshold ε. An important advantage of this definition is that the quantity is non-dimensional (i.e. using diameter of the phase-space), thus ensuring that all values fall between 0 and 1. Another feature of Eq. 5 is that C_2 is a quantitative measure of recurrence, in so far as it identifies, in an average sense, the proportion of time over which recurrence occurs (i.e. a *density*). Because no threshold is used explicitly in Eq. 5, this is referred to as *unthreshold RP* (URP).

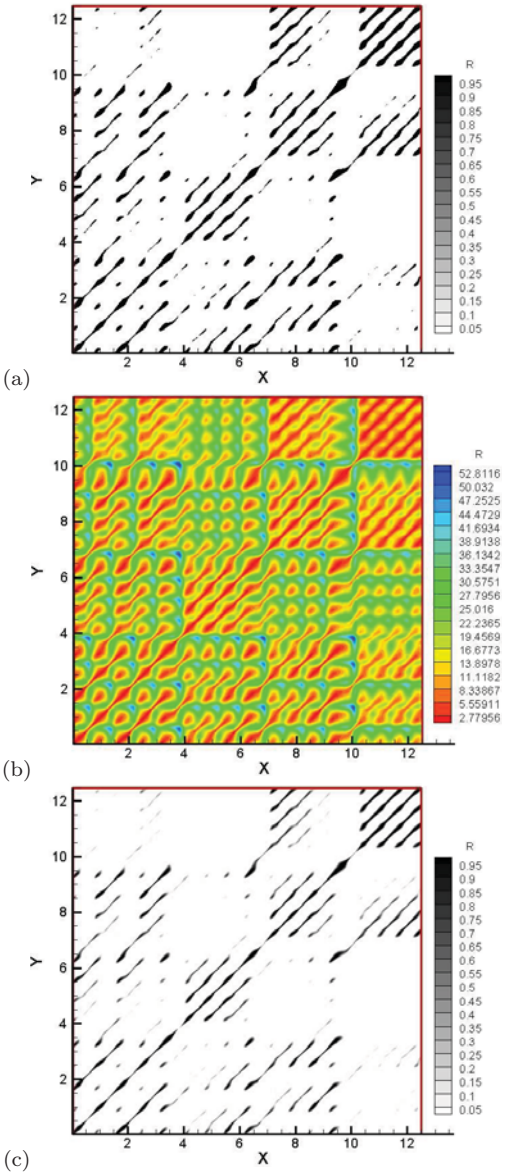

Figure 2: Lorentz attractor: (a) RP with ε=10% of the phase-space diameter, (b) GRP and (c) URP.

The three RP definitions provided above are illustrated by reference to the famous Lorenz attractor (Lorenz, 1963):

$$\begin{aligned} \dot{a_1} &= \sigma(a_2 - a_1) \\ \dot{a_2} &= \rho a_1 - a_2 + a_1 a_3 \\ \dot{a_3} &= -\beta a_3 + a_1 a_3 \end{aligned} \tag{7}$$

where σ, ρ and β are constant. The phase-space trajectory for this system is shown in Fig. 1. The trajectory is characterised by two lobes, each formed by closely-bunched loops. After a number of loops, the dynamical system experiences a drastic change, with the trajectory forming the other lobe. Both the loops and the drastic (cyclic) change of lobes are clearly brought out in the three types of recurrence plots defined earlier and shown in Fig. 2, with diagonal segments identifying *periodic* looping and blocks of lines identifying the lobes (see Lardeau et al., 2008, for more interpretations on the different patterns observed on the RPs).

A second quantitative measure is the *probability of recurrence*. Again, for a given threshold ε and for a time interval τ, this is defined as:

$$p(\varepsilon,\tau) = \frac{1}{N-\tau}\sum_{i=1}^{N-\tau}\theta(\varepsilon - ||\vec{x}^i - \vec{x}^{i+\tau}||) \qquad (8)$$

A more general interpretation is one in which any of RP definitions, Eqs. 3, 4 and 5, replaces the argument under the sum in Eq. 8, thus giving:

$$p(\tau) = \frac{1}{N-\tau}\sum_{i=1}^{N-\tau} O_{i,i+\tau} \qquad (9)$$

with $O_{i,i+\tau}$ being either $R_{i,i+\tau}$, $D_{i,i+\tau}$ or $U_{i,i+\tau}$.

For the Lorenz system, Eq. 5 and Fig. 2, Fig. 3 shows the behaviour of the Probability of Recurrence obtained for the three definitions of RP. The distinct peaks for RP and UPR represent respective lobes in Fig. 2, and the cyclicity (transition from one lobe to another) can be quantified in temporal terms. For the GRP, the variation is less clear, because the continuous gray shading goes hand-in-hand with continuous and relatively weak variations in the probability curve.

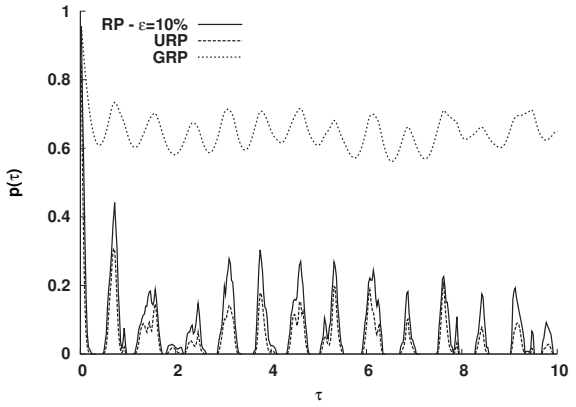

Figure 3: Probability of recurrence, Eq. 9, for the Lorenz attractor.

APPLICATION TO SEPARATED FLOW

This paper restricts itself to an examination of the characteristics of two closely related flows computed with LES by Avdis et al (2009); Fig. 4 shows related instantaneous snapshots. Results for other flows investigated are reported elsewhere. The emphasis is here not, principally, on the physics of separation, but on the extraction of characteristic unsteady features by means of the RP method, in contrast to conventional time-series analysis. Both flows separate from an identical, nominally two-dimensional, dune-shaped hump in a tunnel. They differ by the presence or absence of a thin synthetic (zero-mass) slot jet, extending across the entire spanwise extent and located close to the position at which the flow separates from the hump wall. The effects of the injection are clearly visible in Fig. 4. Both cases correspond to laboratory configurations examined experimentally by NASA (Greenblatt et al., 2005) in the context of separation control (i.e. reduction) with synthetic jets. The juxtaposition of the two flows allows interesting differences

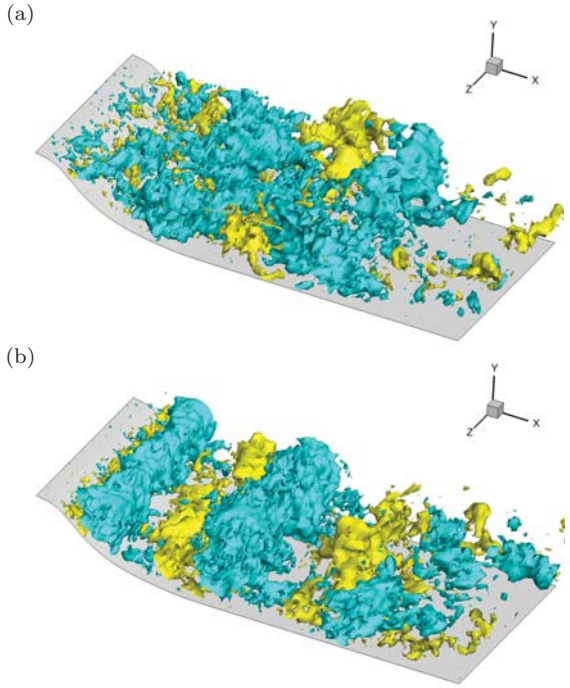

Figure 4: Isosurfaces of vertical velocity for (a) the baseline flow and (b) with zero-net mass injection.

n	q	m	E_n/E_{tot}	n	q	m	E_n/E_{tot}
1	1	1	0.04757805	9	6	1	0.01063542
2	2	1	0.02617285	10	2	2	0.00860705
3	3	1	0.01888331	11	7	1	0.00776091
4	4	1	0.01688989	12	3	2	0.00713798
5	1	2	0.01234243	13	8	1	0.00672639
6	5	1	0.01211669	14	4	2	0.00644351
7	1	0	0.0114942	15	3	0	0.0064337
8	2	0	0.01097353	16	9	1	0.00622801

Table 1: Relative energy associated with the first 16 POD/Fourier modes - Baseline Case.

to be brought out, in respect of the temporal behaviour, as a consequence of the presence or absence of the periodic jet injection. The injection in the perturbed case is at a hump-height-based Strouhal number, $St_h = fh/U_{ref} = 0.2$ - equivalent to the chord-based Strouhal number, $St_C = fC/U_{ref} = 1.66$ – and the Reynolds number, based on chord length and free-stream velocity is close to 1 million. Simulations were performed with a grid of $(768 \times 96 \times 128)$ nodes. The POD decomposition was performed on a 3D sub-domain extending from the wall to $y = 0.2L$ in the wall-normal direction, across the entire spanwise extent of the simulation, and from $x = 0.6L$, just upstream of the mean separation line, to $x = 1.5L$, well downstream of the mean reattachment, which is located at $x = 1.1L$. The POD modes are computed using 2200 snapshots regularly sampled over 28 time units (based on the free-stream velocity and hump length).

RESULTS

The main purpose of the paper is to demonstrate that the RP method allows information to be obtained that cannot be readily derived from conventional time-series analyses. This is done below by contrasting RP results with the spectra

n	q	m	E_n/E_{tot}	n	q	m	E_n/E_{tot}
1	1	1	0.07488363	9	6	1	0.01176285
2	1	0	0.06935005	10	1	2	0.01005792
3	2	0	0.06876842	11	7	1	0.01003761
4	2	1	0.06102749	12	8	1	0.00804597
5	3	1	0.03447086	13	2	2	0.00645995
6	4	1	0.02939622	14	9	1	0.00643326
7	5	1	0.0146129	15	10	1	0.00588129
8	3	0	0.01260445	16	11	1	0.00467147

Table 2: Relative energy associated with the first 16 POD/Fourier modes - Zero-net mass injection.

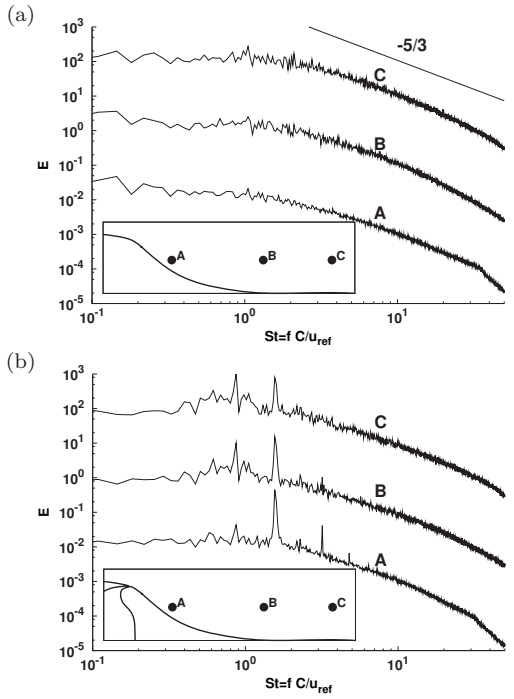

Figure 5: Energy spectra and localisation of the probes for (a) baseline case and (b) zero-net mass injection.

shown in Fig. 5, the upper set being for the baseline flow and the lower one for the jet-actuated flow. The former reveal no distinct frequency peaks or ranges which might indicate cyclicity. However, the latter contain peaks at the injection frequency, $St_C = 1.66$, and another at roughly 0.83. Attention is now turned to the POD and RP results.

Fig. 6 gives the time variation of the first 16 POD coefficients, for both flows shown in Fig. 4. Two corresponding sets of 8 selected POD mode shapes are shown in Figs. 7 and 8, respectively. URPs for the two cases are shown in Fig. 9, the last constructed with the leading 16 modes, containing 20% and 43% of the fluctuating energy for the baseline and jet-actuated cases, respectively. Tables 1 and 2 - relating to the baseline and perturbed flows, respectively give the mode-related distribution of energy as a fraction of the total value. In the tables, q is the quantum number (see Eq. 2) and m is the number of full waves in the homogeneous direction, corresponding to the wave number $k = 2\pi m/L_z$ contained in Eq. 2. The relevance of m becomes obvious if considered against the mode shape in Fig. 7 and 8. Thus, for example, for mode $n = 5$ in Table 1, $m = 2$, and Fig. 7(c) shows that this corresponds to two complete spanwise waves in the mode shapes. A discussion of the physical implica-

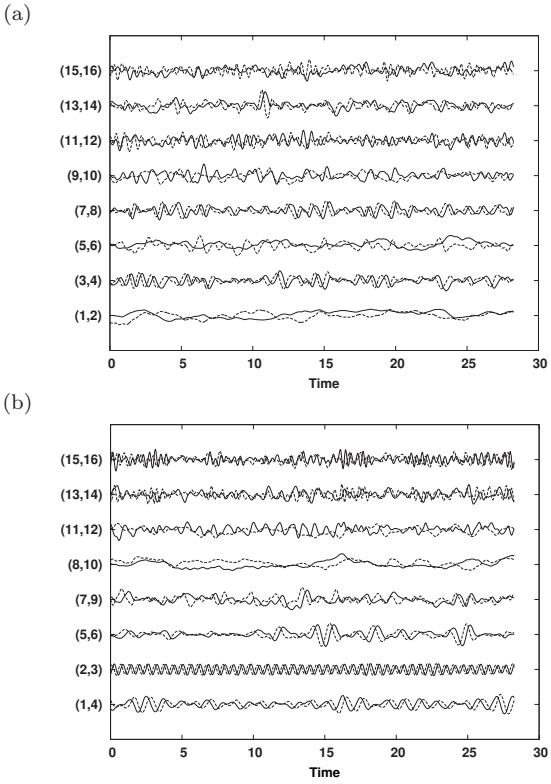

Figure 6: Temporal evolution of the first 16 modes, paired by level of energy for (a) the baseline flow and (b) with zero-net mass injection.

tions of the mode shape is given in Avdis et al (2009). One facet of this interpretation is that the structure of baseline case is dominated by streamwise-elongated features, indicative of streamwise-oriented vortices, relative to clumpy and spanwise homogeneous features in the actuated case, associated with the injection and its interaction with (break-up of) the streamwise-oriented vortices. This discussion is not pursued further herein. Rather, attention is turned to the temporal behaviour.

For the baseline flow, the temporal evolution of the coefficients for modes n =1 and 2 (Fig. 6a) give no hint of a periodic behaviour. At a lower energy level, modes n =7 and 8 appear to reflect a Kelvin-Helmholtz-type shedding, an inference derived from the associated $m = 0$ mode shape, Fig. 7(e). The temporal coefficients of these latter modes feature recurrent, nearly periodic intervals, of length of order 1.2 time units corresponding to a Strouhal number St_C=0.83 (i.e. about 0.5 times the injection frequency. There is also an indication of a much lower-frequency modulation in n =7 and 8, with a period of roughly 5 time units (i.e. $St_C = 0.2$). A similar modulation is also visible in modes n =2 and 3, suggesting the possibility of cyclic behaviour.

In the perturbed case, the temporal coefficients of modes n=2 and 3, these being associated with the injection-induced flapping, show the expected strongly pronounced sinusoidal behaviour, consistent with the periodic injection process. Mode n=2 is shown in Fig. 8(b), and this is characterized by spanwise homogeneous features ($m = 0$). Table 2 shows this mode to be almost as energetic as mode n =1, suggesting that the streamwise-oriented features in this mode of the baseline case are still present, albeit distorted by the injection. Higher modes are associated with lumpy structures that are convected, as in the unperturbed case, above and

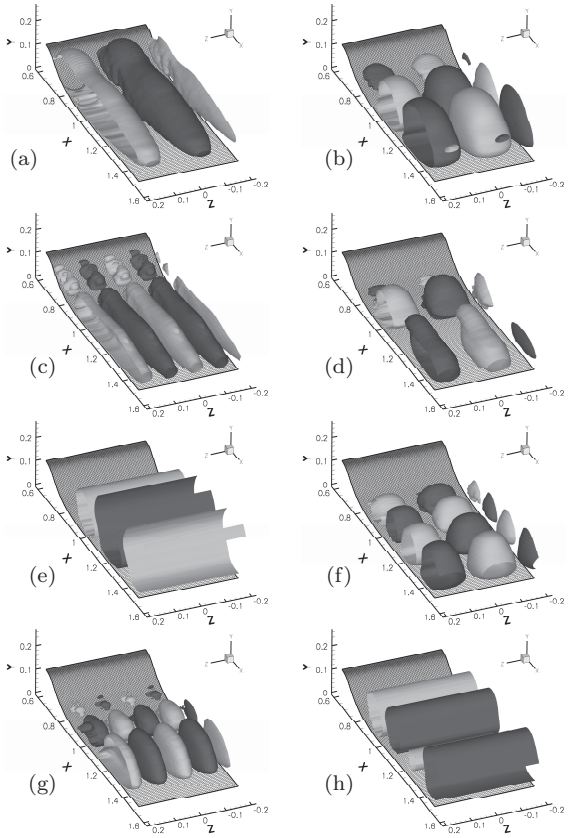

Figure 7: Isosurfaces of $\phi_2^n(x,y,z) = \pm 0.2$ for (a) $n = 1$, (b) $n = 3$, (c) $n = 5$, (d) $n = 6$, (e) $n = 7$, (f) $n = 11$, (g) $n = 12$ and (h) $n = 15$.

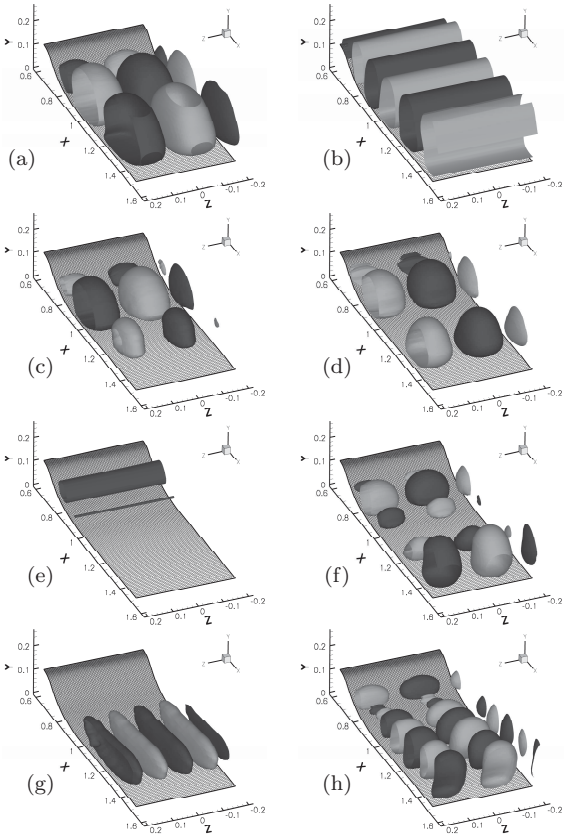

Figure 8: Isosurfaces of $\phi_2^n(x,y,z) = \pm 0.2$ for (a) $n = 1$, (b) $n = 2$, (c) $n = 5$, (d) $n = 7$, (e) $n = 8$, (f) $n = 11$, (g) $n = 13$ and (h) $n = 15$.

within the separated region. Their temporal coefficients give a hint of cyclicity in the system, but the evidence gleaned purely from the modes is very indistinct.

The URP for the baseline case (Fig. 9a) shows little evidence of periodicity - i.e. there are very few lines parallel to the LOI that are distinguishable as such - but there is clear evidence of cyclicity, wherein the system executes short-periods recurrent events that are represented by dark square patches, e.g. between $T = 7$ and 12. Thus, the predominant features in the URP are vertical and horizontal stripes, with a period varying between 3 and 5 time units, corresponding to $St_C = 0.25$. The RP for the perturbed case is much more structured. First, it provides clear evidence of the periodic injection process by way of the streaks parallel to the LOI, which are separated by about 0.5 time units, corresponding to the Strouhal number of the injection, $St_C = 1.66$, corresponding to modes n =2 and 3, Fig. 6(b). Second, the URP shows thick lines parallel to the LOI, which are separated by about one time unit. Third, it features a cyclic behaviour, similar to that in the baseline case, but with a considerably longer time scale of around 10 time units. In a sense, it may be said that one effect of the periodic injection is to reduce the complexity of the dynamical system, by reducing the number of significant modes. While the injection destabilizes the first two modes of the unperturbed flow, the system continues to undergo major changes in state at a time scale more than one order of magnitude larger than that of the injection process. This cyclicity is virtually impossible to derive from the POD information alone, and hence this case illustrates well that RPs can provide useful information which is, at best, very difficult to derived from conventional analytical tools, as discussed by reference to the spectra in Fig. 5.

Figure 10 shows distributions for the Probability of Recurrence, both derived from the URPs applied to the baseline and perturbed flows, respectively. Each plot contains three curves: one is derived by using all modes in Tables 1 and 2, the second is derived by combining only modes having $m = 0$, and the third by combining only modes having $m = 1$. The purpose is to attempt to bring to the fore the type of spanwise modes that are associated with the cyclic behaviour observed in the URPs themselves. For the baseline flow, the Probability plot strongly suggests a cyclicity of duration of roughly 5 time units (about eight times the injection period), associated with $m = 1$ modes. These modes correspond to a spanwise pair of streamwise elongated mode shapes, and the implication is that the cyclicity arises from alternating faster/slower moving spanwise structures. In accord with the above, the comparison of the two plots in Fig. 10 shows that the "frequency" corresponding to 5 time units is indeed roughly 0.12 times the jet-injection frequency. The latter is brought out by the $m = 0$ modes that identify the spanwise homogeneous jet injection. A further conclusion derived from Fig. 10 is that the $m = 1$ cyclicity, observed in the baseline flow, is barely noticeable when injection is introduced. Instead, the $m = 1$ modes indicate the presence of a near-periodic feature of duration roughly twice the injection period (i.e $St_C = 0.83$, *cf.* Fig. 5). This feature is also recognised from the URP as being represented by the thicker black lines aligned with the LOI. Thus, the injec-

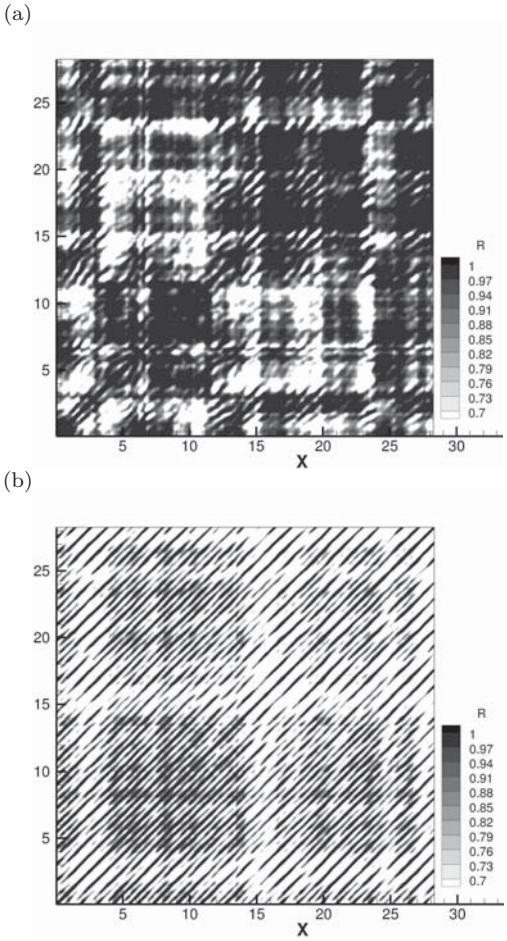

Figure 9: URP for (a) the baseline flow and (b) with zero-net mass injection, for all cases using the first 16 most energetic modes.

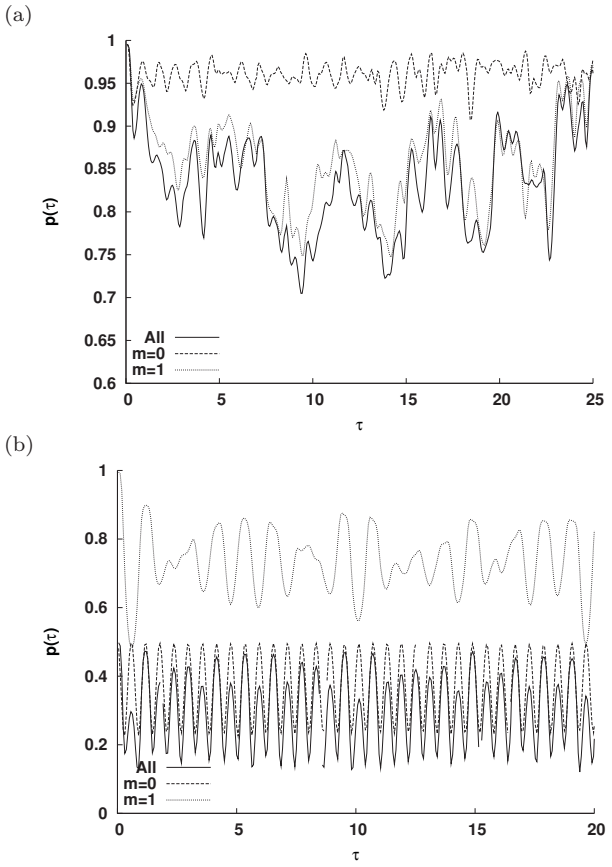

Figure 10: Probability of recurrence $p(\tau)$, using unthresholded recurrence plots for (a) baseline case and (b) zero-net mass injection.

tion substantially weakens the cyclic slower/faster moving spanwise structures as well as increasing their frequency.

CONCLUSIONS

Periodic and cyclic events in two related turbulent flows separating from a nominally 2-d hump, one being a periodically perturbed version of the other, are investigated using a combination of POD and Recurrence Plot (RP) analysis. To the authors' knowledge, this is the first time that this type of analysis is performed on fully turbulent flow fields. For the unperturbed baseline flow, the RP analysis reveals motions with two preferential time-scales that cannot be detected in spectra: a low-frequency motion ($St_C = 0.2$) presumed to be associated with cyclically-varying streamwise-elongated structures, and a higher-frequency motion ($St_C = 0.83$) presumed to identify KH instability in the separated shear layer. For the case perturbed by the synthetic jet at $St_C = 1.66$, two dominant frequencies observed in the related spectra are also brought out in the RPs and especially in the Probability of Recurrence variations. However, only the RP analysis allows the presence of spanwise-homogeneous structures, associated with the injection frequency, to be separated from the streamwise-elongated structures at the frequency $St_C = 0.83$. Moreover, only the RP reveals the long-time-scale cyclicity also observed in the baseline case, although it is much weaker in the perturbed flow. This type of analysis is currently being applied to other flows, among them separation from a 3-d hill and free shear flows. The analysis can also be used to identify spurious long-time-scale periodicity rooted in numerical artefacts and looped precursor data for shear flow fed into the flow-inlet planes of LES domains.

REFERENCES

Avdis, A., Lardeau, S. & Leschziner, M.A., 2008. "Large eddy simulation of separated flow over a two-dimensional hump with and without control by means of a synthetic slot-jet". *Flow, Turb. and Comb*, to appear.

Greenblatt, D., Paschal, K., Yao, C. & Harris, J., 2006, "A separation control cfd validation test case part 2. zero-efflux oscillatory blowing". *AIAA paper*, 2005-485.

Holmes, P., Lumley, J.L. & Berkooz, G., 1996, *Turbulence, Coherent Structures, Dynamical Systems and Symmetry.* Cambridge University Press.

Lardeau, S., Tessicini, F. & Leschziner, M.A., 2008, "Analysis of cyclic events in turbulent flows by means of recurrence plots". *Phys. Fluids*, submitted.

Lorenz, E.N., 1963, "Deterministic nonperiodic flows". *J. Atmos. Sc.* 20, 130141.

Marwan, N., Romano, M.C., Thiel, M. & Kurths, J., 2007, "Recurrence plots for the analysis of complex systems". *Physics Reports* 438, 237329.